

Strömgren metallicities for intermediate-age and old star clusters

Andrés E. Piatti^{1,2*}

¹ Instituto Interdisciplinario de Ciencias Básicas (ICB), CONICET-UNCUYO, Padre J. Contreras 1300, M5502JMA, Mendoza, Argentina;

² Consejo Nacional de Investigaciones Científicas y Técnicas (CONICET), Godoy Cruz 2290, C1425FQB, Buenos Aires, Argentina

Received / Accepted

ABSTRACT

We report results that show that the straightforwardly star cluster metallicities obtained from Strömgren vby photometry is age-dependent and need to be corrected for further use. This outcome arises from the comparison of $[Fe/H]$ values derived from Strömgren photometry with those metallicities published in the literature for 26 Large and Small Magellanic Cloud star clusters, whose ages range from ~ 1 Gyr up to the known oldest globular clusters' ages in these galaxies. While deriving mean star cluster metallicities we carried out a thorough selection of red giant branch candidates to comply with the Strömgren metallicity calibration validity regime. We paid attention to the effect of contamination by field stars, particularly of those that lie inside the star clusters' radii, distributed along the star cluster red giant branches, and with $[Fe/H]$ values covering a similar range as that for the selected stars. We found that the measured Strömgren metallicities are systematically more metal-poor than the published ones and that a quadratically age-varying function reproduces the relative metallicity values with an overall uncertainty of ~ 0.05 dex. We finally performed a similar comparison relying on a fully independent approach, that consisted in using theoretical red giant branches of old globular clusters spanning $[Fe/H]$ values from -2.0 up to 0.0 dex as standard ones. We then superimposed on to them the red giant branches of star clusters with ages in the range $1.0 - 12.5$ Gyr and estimated by interpolation their associated metallicities. The derived theoretical relative metallicities follow a similar trend as a function of the star clusters' ages than that found from observations of star clusters.

Key words. Methods: observational - techniques: photometric - globular clusters: general - open clusters and associations: general - stars: abundances

1. Introduction

Star clusters' metallicities have long been used as key parameters for unveiling the chemical evolution of galaxies. Their metal abundances tell us about the efficiency of the gas mixing within a galaxy, the metal enrichment along the galaxy lifetime, the infall of gas from galaxy interactions, etc. Alongside with ages and positions (age-metallicity relationships, metallicity gradients), star clusters' metallicities have helped us with understanding whether galaxies formed through outside-in or inside-out formation scenarios, detecting the existence of bursting formation episodes that produced a sudden chemical enrichment, estimating the effectiveness of scattering star clusters, among others.

In this context, the red giant branch of old star clusters has been employed to estimate metallicities from a variety of photometric systems, namely: Johnson BV (Hartwick 1968), Johnson-Cousins VI (Da Costa & Armandroff 1990), Washington CT_1 (Geisler & Sarajedini 1999), near-IR J, K_s bands (Frogel et al. 1983), etc. This is because the colors of the red giant branch stars show sensitivity to changes in metallicities. The result is that the red giant branches appear shifted towards bluer regions in the color-magnitude diagram (CMD) as the star clusters are more metal-poor. In practice, a fixed magnitude level is adopted and the color differences at that magnitude level is obtained and transformed into $[Fe/H]$ values. Nevertheless, having a long and well-populated red giant branch is advantageous, since it can be superimposed on to the standard iso-abundance red giant

branches and thus to obtain by interpolation a metallicity estimate.

These iso-abundance red giant branches have usually been drawn from CMDs of old globular clusters, so that when using them for estimating metallicities of younger star clusters, the derived $[Fe/H]$ values result much more metal-poor because of the age-metallicity degeneracy. This phenomenon has been studied from numerical simulation for the Johnson VI photometric system by Ordoñez & Sarajedini (2015), who showed that the metallicity derived from the star cluster's red giant branch stars can be in error by up to ~ 0.5 dex, if the star cluster is younger than ~ 6 Gyr old. Geisler et al. (2003) also derived an age-dependent metallicity correction for the Washington CT_1 photometric system, which shows that $[Fe/H]$ values of star clusters of ~ 1 Gyr old need to be corrected by ~ 0.7 dex in order to compute reliable metallicities.

The Strömgren vby medium-bandwidth filters (Crawford & Mandwewala 1976) have proved to be able to derive straightforwardly accurate metallicities values ($[Fe/H]$) for many stars in a star cluster field, provided the photometric data are precise (see, e.g., Frank et al. 2015; Massari et al. 2016; Gruyters et al. 2017). This is because of the index $m_1 = (v - b) - (b - y)$ has resulted to be a metallicity-sensitive one, as judged by the available calibrations of it as a photometric proxy of iron abundances. Particularly, the semi-empirical calibration obtained by Calamida et al. (2007) has turned out to be the most robust one for estimating metallicities of red giants (Adén et al. 2009; Calamida et al. 2009; Árnadóttir et al. 2010). It was derived using high-dispersion spectroscopic data of red giants of Milky

* e-mail: andres.piatti@unc.edu.ar

Way globular clusters and alpha-enhanced isochrones transformed to the observational plane by using semi-empirical color-temperature relations.

In this work, we present Strömgren vby photometry of intermediate-age Large and Small Magellanic Cloud (LMC/SMC) star clusters aiming at investigating at what extend the Strömgren metallicities are affected by the age-metallicity degeneracy. If such a age-metallicity dependence exists, it should arise from the comparison of the metallicities measured here from the Strömgren indices with those accurate values available in the literature. The paper is organized as follows: Section 2 introduces the obtained Strömgren vby images and describes their processing until obtaining the standardized photometric data sets. Sections 3 and 4 deal with the metallicity estimates and the aforementioned age-metallicity correction. Finally, Section 5 summarizes the main results of this work. We note that a metallicity calibration based on young stellar evolutionary models would be of great value. Such a calibration would consider the different evolutionary status of young stars (~ 1 Gyr) compared to old stars (> 10 Gyr) in different Strömgren colors' planes.

2. Strömgren photometric data

We made use of Strömgren vby images collected during the observing program SO2008B-0917 (PI: Pietrzyński), conducted with the SOAR Optical Imager (SOI) attached to the 4.1m Southern Astrophysical Research (SOAR) telescope (FOV = $5.25' \times 5.25'$, scale = $0.154''/\text{px}$ in binned mode). The observing program was executed during two different epochs (17-19 December 2008 and 16-18 January 2009) under excellent image quality conditions (typical FWHM $\sim 0.6''$). We downloaded the observational material from the National Optical Astronomy Observatory (NOAO) Science Data Management (SDM) Archives.¹ Table 1 lists the log of observations for the studied LMC/SMC star clusters.

We processed the images following the SOI's reduction prescriptions available at <http://www.ctio.noao.edu/soar/content/soar-optical-imager-soi>, so that we also used nightly zero and flat-field images. As for the photometry standardization, we employed observations of the following Strömgren standard stars: HD64, HD3417, HD12756, HD22610, HD57568, HD58489, HD66020, TYC 7547-711-1, TYC 7548-698-1, TYC 7583-1011-1, TYC 7583-1622-1, TYC 7626-763-1, TYC 8033-906-1, TYC 8067-207-1, TYC 8104-856-1 and TYC 8104-969-1 (Hauck & Mermilliod 1998; Paunzen 2015). They were observed in all the vby filters at airmass spanning the range $\sim 1.02 - 2.20$. Standard stars were observed at a fixed airmass twice to allow them to be placed in the two different CCDs arrayed by SOI, and thus to monitor their individual responses. Piatti & Bailin (2019) showed that the transformation coefficients obtained from magnitudes of standard stars placed in each CCD are indistinguishable, so that we enlarged the sample of standard star magnitude measurements by considering all of them irrespective of their positions in SOI. To convert instrumental magnitudes into standard ones, we first gathered all the information of the standard stars, and then fitted the following expressions:

$$v = v_1 + V_{\text{std}} + v_2 \times X_v + v_3 \times (b - y)_{\text{std}} + v_4 \times m_{1\text{std}}, \quad (1)$$

¹ <http://www.noao.edu/sdm/archives.php>.

$$b = b_1 + V_{\text{std}} + b_2 \times X_b + b_3 \times (b - y)_{\text{std}} \quad (2)$$

$$y = y_1 + V_{\text{std}} + y_2 \times X_y + y_3 \times (b - y)_{\text{std}}, \quad (3)$$

where v_i , b_i and y_i are the i -th fitted coefficients, and X represents the effective airmass. The resulting mean transformation coefficients are listed in Table 2 of Piatti et al. (2019), who used images from the same observing program to estimate metallicities of young star clusters in the LMC/SMC from their supergiant populations.

We relied on the routine packages DAOPHOT, ALLSTAR, DAOMATCH and DAOMASTER (stand-alone version, Stetson et al. 1990) to obtain point-spread-function (PSF) photometric data sets of the star clusters' fields and their associated uncertainties. In order to build the PSF of an image, we first interactively selected nearly one hundred well-isolated, relatively bright, not-saturated stars, distributed over the whole image area. A subsample of the nearly best forty PSF stars was used to build a preliminary PSF, that was applied to the image aiming at cleaning the entire PSF star sample from fainter neighbors. With the cleaned PSF stars, we constructed the final quadratically spatially-varying PSF for that image and computed aperture corrections that resulted in the range $-0.04 - -0.07$ mag. The PSF was applied to the entire list of identified stellar sources in the image. The resulting subtracted image was employed to identify new ones, which were fitted by the PSF simultaneously with those in the previous list. We took advantage of this procedure of enlarging the photometrically measured star sample by iterating it three times. Their standard magnitudes were obtained by inverting eqs. (1)-(3) and by entering with the computed instrumental magnitudes. The above described procedure was repeated for each of the images listed in Table 1. In the subsequent analysis, we only kept those stellar sources with $\chi < 2$ and $|\text{SHARPNESS}| < 0.5$. χ is a DAOPHOT robust estimate of the ratio: the observed pixel-to-pixel scatter from the model image profile divided by the expected pixel-to-pixel scatter from the image profile (see Figure 28 in Stetson & Harris 1988), while SHARPNESS is another image quality diagnostic defined as the ratio of the height of the bivariate delta-function which best fits the brightness peak in the original image to the height of the bivariate Gaussian function which best fits the peak. We adopted the frequently used values of χ and SHARPNESS to exclude bad pixels, cosmic rays, galaxies and unrecognized double stars.

In order to quantify the uncertainties associated to the obtained photometry we followed the recipe applied in previous studies of other subsets of star clusters observed during the same observing program (see Piatti & Koch 2018; Piatti 2018). The method consists in adding to an image synthetic stars with magnitudes and positions distributed similarly to those of the measured stars, and carrying out the photometry for the new image as described above. The synthetic stars represent nearly 5% of the measured stars, so that the original image stellar density is not significantly altered. The resulting magnitudes for the synthetic stars are then compared with those used to create such stars. The difference between them turned out to be typically equal to zero and in all the cases smaller than 0.003 mag. We then decided to use as photometric errors the rms errors obtained from the comparison of input and output synthetic star magnitudes.

Table 1. Observing log and properties of the LMC/SMC star cluster sample.

Star cluster ^a	Date	Exp. time (sec)			Airmass			$E(B - V)$ (mag)	Age (Gyr)	Ref.	$[\text{Fe}/\text{H}]_{\text{adopted}}$ (dex)	$[\text{Fe}/\text{H}]$ (dex)
		v	b	y	v	b	y					
LMC												
NGC 1651	2008-12-18	500	200	120	1.54	1.53	1.53	0.07	2.00±0.20	1,2	-0.70±0.10	-1.05±0.15
NGC 1795	2008-12-19	350	140	90	1.38	1.38	1.37	0.07	1.50±0.20	4,5	-0.40±0.10	-0.90±0.15
NGC 1846	2008-12-18	500	200	120	1.61	1.60	1.59	0.07	1.40±0.20	2,6	-0.50±0.10	-0.90±0.15
NGC 2155	2008-12-18	500	200	120	1.37	1.36	1.36	0.04	3.00±0.30	1,3	-0.70±0.10	-1.00±0.10
SL 8	2009-01-16	350	180	100	1.33	1.34	1.34	0.07	1.80±0.30	7	-0.40±0.20	-0.85±0.10
SL 363	2008-12-17	300	100	60	1.46	1.45	1.44	0.07	2.24±0.10	2	-0.49±0.12	-0.90±0.15
SL 388	2009-01-16	350	140	90	2.04	2.02	2.01	0.04	2.20±0.30	7	-0.65±0.20	-0.95±0.10
SL 509	2008-12-19	350	140	90	1.46	1.46	1.45	0.05	1.20±0.30	7	-0.54±0.09	-1.10±0.15
SL 549	2009-01-18	350	140	90	1.84	1.83	1.82	0.05	1.70±0.30	8	-0.70±0.20	-1.10±0.10
SL 555	2009-01-18	350	140	90	1.79	1.81	1.82	0.07	1.70±0.20	9	-0.70±0.20	-1.10±0.10
SL 817	2009-01-17	450	180	110	2.12	2.10	2.08	0.07	1.50±0.30	7	-0.41±0.05	-0.95±0.10
SL 842	2009-01-18	400	180	100	2.01	2.06	2.09	0.05	2.20±0.30	7	-0.60±0.20	-1.00±0.10
SL 862	2009-01-18	400	180	100	2.04	2.02	2.02	0.07	1.80±0.30	7	-0.47±0.07	-0.90±0.15
SMC												
L 6	2008-12-17	500	300	180	1.91	1.89	1.88	0.03	3.30±0.70	10	-1.07±0.17	-1.25±0.20
L 19	2008-12-18	500	300	180	1.51	1.50	1.50	0.03	2.10±0.20	10	-0.75±0.10	-1.05±0.15
L 27	2008-12-18	500	300	180	1.46	1.45	1.44	0.03	2.10±0.20	10	-1.14±0.06	-1.50±0.15

^a Star cluster identifications are from Shapley & Lindsay (1963, SL) and Lindsay (1958, L).

Ref. : (1) Kerber et al. (2007); (2) Goudfrooij et al. (2014); (3) Piatti & Bastian (2016); (4) Correnti et al. (2014); (5) Glatt et al. (2010); (6) Piatti (2011b); (7) Bica et al. (1998); (8) Piatti et al. (2003); (9) Geisler et al. (2003); (10) Piatti et al. (2005).

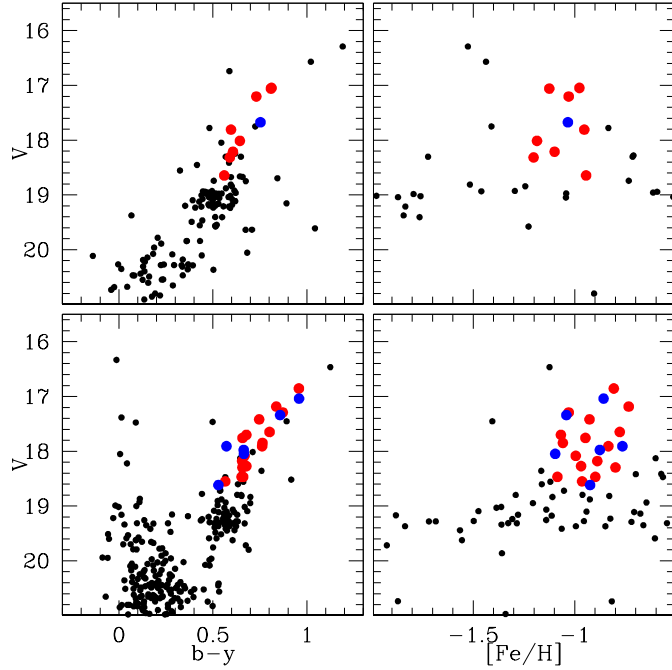


Fig. 1. V vs. $b - y$ CMD for measured stars distributed inside the star cluster's radius (left panel) and their metallicity ($[\text{Fe}/\text{H}]$) distribution as a function of the V magnitude (right panel). Red and blue large filled circles represent stars used to compute the star cluster's mean $[\text{Fe}/\text{H}]$ value and those from a reference star field with $[\text{Fe}/\text{H}]$ values similar to those of the star cluster's stars, respectively (see text for details). Top and bottom panels refer to NGC 1651 and 1795, respectively.

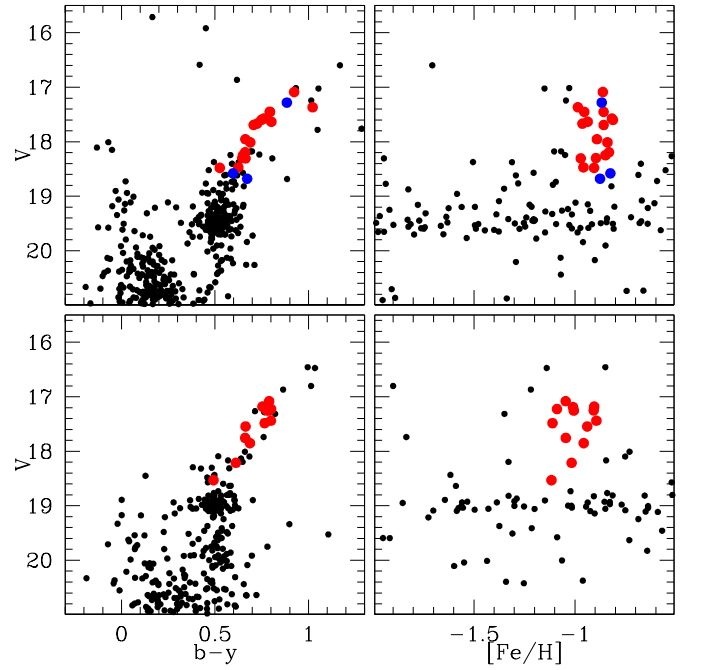


Fig. 2. Same as Figure 1, for NGC 1846 (top panels) and 2155 (bottom panel).

3. Metallicity estimates

The metallicity calibration obtained by Calamida et al. (2007) involves the m_{10} and $(v - y)_0$ indices of red giant branch stars, corrected by reddening, according to the following expression:

$$m_{10} = \alpha + \beta[\text{Fe}/\text{H}] + \gamma(v - y)_o + \delta[\text{Fe}/\text{H}](v - y)_o \quad (4)$$

where $\alpha = -0.309$, $\beta = -0.090 \pm 0.002$, $\gamma = 0.521 \pm 0.001$, and $\delta = 0.159 \pm 0.001$, respectively. While de-reddening color indices

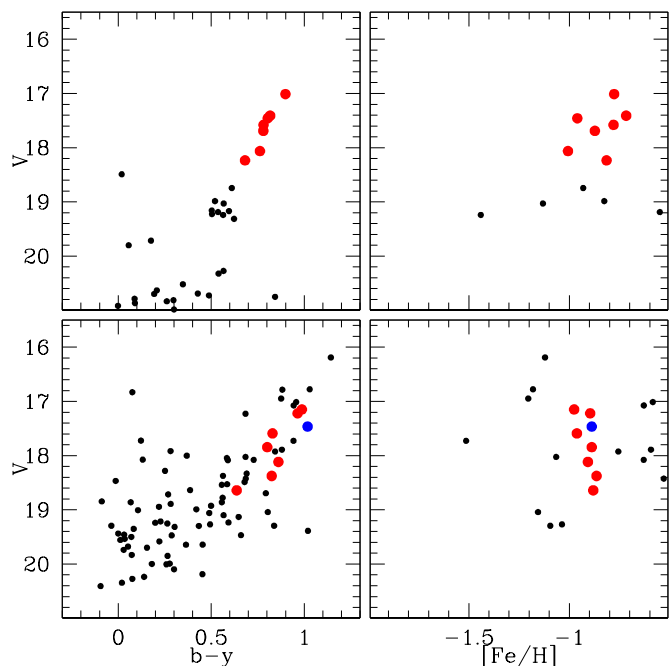


Fig. 3. Same as Figure 1, for SL 8 (top panels) and 363 (bottom panel).

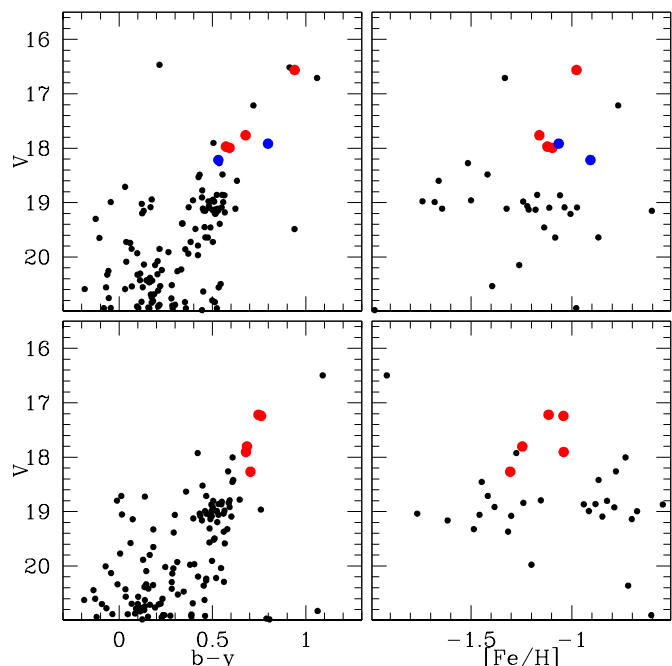


Fig. 5. Same as Figure 1, for SL 549 (top panels) and 555 (bottom panel).

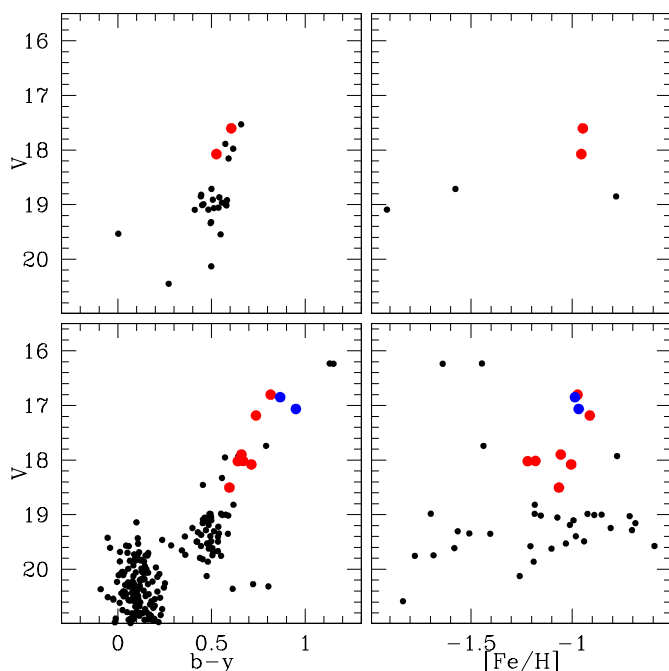


Fig. 4. Same as Figure 1, for SL 388 (top panels) and 509 (bottom panel).

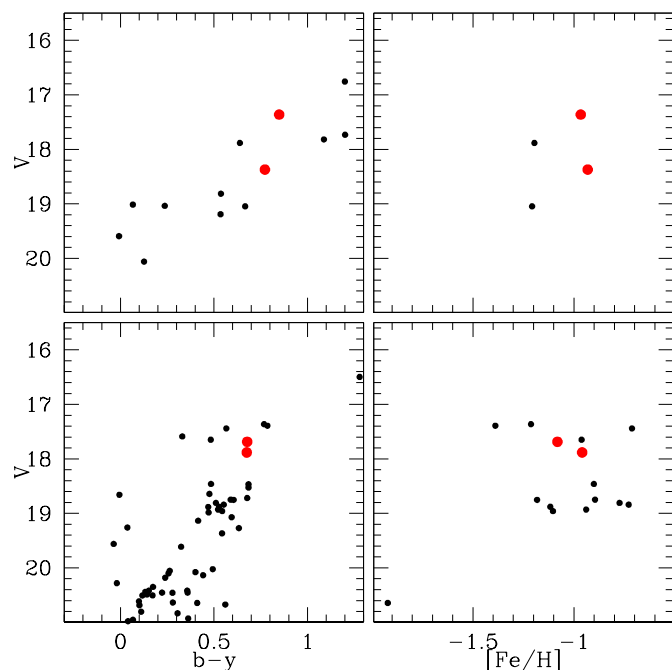


Fig. 6. Same as Figure 1, for SL 817 (top panels) and 842 (bottom panel).

is a somehow straightforward task, the selection of red giant branch stars requires several steps. We retrieved the $E(B - V)$ values obtained by Schlafly & Finkbeiner (2011) from the NASA/IPAC Infrared Science Archive² (see Table 1) using the star clusters' coordinates, and computed the intrinsic colors:

$$(v - y)_0 = (v - y) - 1.67 \times 0.74E(B - V)$$

and

$$m_{10} = (v - b) - (b - y) + 0.33 \times 0.74E(B - V)$$

where the reddening laws, $E(X)/E(B - V)$, with $X = v - y, m_1$, are those given by Crawford & Mandwewala (1976). The $(v - y)_0$ and m_{10} values were then entered in eq. (4) to compute individual stellar metallicities. Their errors were estimated from a full analytical propagation of errors, including those on the

² <https://irsa.ipac.caltech.edu/>

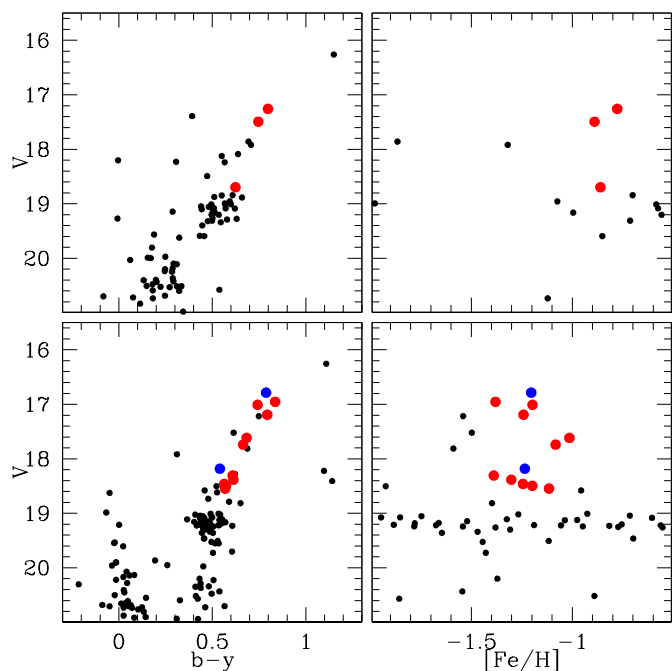


Fig. 7. Same as Figure 1, for SL 862 (top panels) and L 6 (bottom panel).

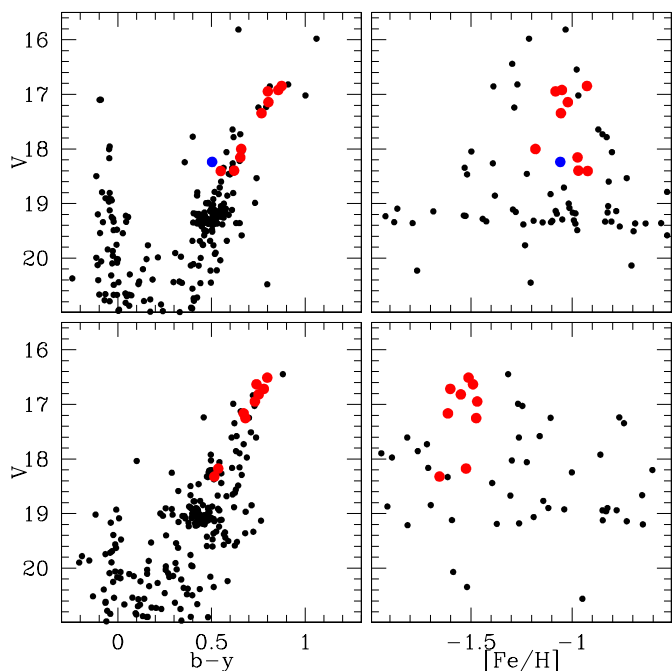


Fig. 8. Same as Figure 1, for L 19 (top panels) and 27 (bottom panel).

calibration coefficients, as follows:

$$\sigma([\text{Fe}/\text{H}])^2 = \left(\frac{\partial[\text{Fe}/\text{H}]}{\partial\alpha}\sigma(\alpha)\right)^2 + \left(\frac{\partial[\text{Fe}/\text{H}]}{\partial\beta}\sigma(\beta)\right)^2 + \left(\frac{\partial[\text{Fe}/\text{H}]}{\partial\gamma}\sigma(\gamma)\right)^2 + \left(\frac{\partial[\text{Fe}/\text{H}]}{\partial\delta}\sigma(\delta)\right)^2 + \left(\frac{\partial[\text{Fe}/\text{H}]}{\partial m_{1o}}\sigma(m_{1o})\right)^2 + \left(\frac{\partial[\text{Fe}/\text{H}]}{\partial(v-y)_o}\sigma((v-y)_o)\right)^2,$$

$$\sigma([\text{Fe}/\text{H}])^2 = \left(\frac{0.002[\text{Fe}/\text{H}]}{c}\right)^2 + \left(\frac{0.001(v-y)_o}{c}\right)^2 + \left(\frac{0.001[\text{Fe}/\text{H}](v-y)_o}{c}\right)^2 + \left(\frac{\sigma(m_{1o})}{c}\right)^2 + \left(\frac{(-0.521c - 0.159(m_{1o} + 0.309 - 0.521(v-y)_o)\sigma(v-y)_o)}{c^2}\right)^2,$$

where $c = -0.090 + 0.159(v-y)_o$, and $\sigma(m_{1o})$ and $\sigma((v-y)_o)$ are the photometric errors in m_{1o} and $(v-y)_o$, respectively. The mean star clusters' metallicities were calculated using the individual $[\text{Fe}/\text{H}]$ values of the selected stars, weighed by their respective uncertainties (see last column of Table 1). We provide in the Appendix A a comparison of the $[\text{Fe}/\text{H}]$ values derived for the selected stars (red filled circles in Figures 1-8) from the semi-empirical calibration with those based on the empirical and theoretical ones, respectively.

Star clusters' red giant branch stars were selected according to the following criteria: (i) The stars are located inside the clusters' radii (Hill & Zaritsky 2006; Bica et al. 2008; Werchan & Zaritsky 2011). This is a basic starting point, because contamination from field stars is also present inside those areas. Furthermore, intermediate-age and old LMC/SMC star clusters are frequently projected toward star fields with similar ages and metallicities (Geisler et al. 2003; Piatti 2011a), which means that they also populate the star cluster CMD regions. (ii) They are distributed along the red giant branch and above the star cluster red clump/horizontal branch in the V versus $b-y$ CMD; $b-y$ is mainly a temperature effective indicator with less metallicity sensitivity (Crawford & Mandwewala 1976). We initially imposed the simple restriction: $V < 18.7$ mag and $b-y > 0.4$ mag (see Figures 1-8, left panels). These magnitude and color cuts still allow several field stars appear not only along the star clusters' red giant branches, but also far away of them. Stars outside the red giant branches were later easily discarded when applying the metallicity cut. (iii) The star clusters' red giant branch stars span a readily visible range of $[\text{Fe}/\text{H}]$ values in the V versus $[\text{Fe}/\text{H}]$ plane. Figures 1-8 (right panels) highlight them with red large filled circles, where all the stars distributed within the star clusters' radii that have a metallicity estimate from eq. (4) are also shown with black dots, irrespective if they are red giant branch stars (see also Appendix C).

While identifying the star clusters' red giant branch candidates we considered the $[\text{Fe}/\text{H}]$ errors ($\sigma[\text{Fe}/\text{H}]$). Figure 9 shows $\sigma[\text{Fe}/\text{H}]$ as a function of V for all the selected stars. As can be seen, the fainter a star the larger $\sigma[\text{Fe}/\text{H}]$. For this reason, we gave more weight to the brightest stars with more accurate photometry and hence with the smallest $[\text{Fe}/\text{H}]$ uncertainties. Likewise, as the V magnitude increases, both $\sigma[\text{Fe}/\text{H}]$ and the dispersion of the individual $[\text{Fe}/\text{H}]$ values increase, because of the poorer photometry quality, so that the observed $[\text{Fe}/\text{H}]$ range of the brightest selected stars more properly reveals the star cluster metallicity range. This metallicity range should be the same at any magnitude level. We also beared in mind that stars distributed along or adjacent to the star clusters' red giant branches could be field stars with ages difference from those of the star clusters (and hence difference metallicities). These stars spuriously produce a wider spread of $[\text{Fe}/\text{H}]$ values for relatively bright V magnitudes. The combined population of field and star cluster red clump stars also produce wide ranges of $[\text{Fe}/\text{H}]$ values. Here

we did not use those stars and kept them in Figures 1-8 for illustrative purposes.

4. Analysis

We evaluated the degree of contamination by field stars in the resulting mean star cluster metallicities. We are interested in those stars that lie along the star clusters' red giant branches and also have metallicities close to the star clusters' values. These stars play a role when computing the mean star cluster metallicities, because we cannot distinguish them from star clusters' stars without the availability of proper motions or radial velocities. We used different equal star clusters areas located reasonably far from the star clusters and counted the number of stars (N_{field} , represented with blue filled circles in Figures 1-8) distributed inside them that satisfy the criteria required for the selected red giant branch stars (N_{cls}). We then computed the ratio N_{field}/N_{cls} and built Figure 10, which depicts its variation as a function of N_{cls} . As can be seen, half of the star cluster sample is affected by a mean null field star contamination. SL 549 amounts 50% of contribution from field stars in the derived mean metallicity. Nevertheless, Figure 5 (right panel) shows that this is because of the small number of stars used. These field stars could increase the standard deviation up to ~ 0.03 dex, the mean metallicity value would not change. A similar interpretation could be applied to the remaining stars clusters, where the smaller the N_{field}/N_{cls} ratio, the smaller the increase of the respective standard deviation.

We searched the literature for ages and metallicities of the studied star cluster sample. Appendix B deals with the individual values available in the literature, while the adopted values are listed in Table 1. From that piece of information (see Table B.1) we computed the difference between the individual reference star clusters' metallicities and the values derived in this work, distinguishing those coming from high- or low-resolution spectroscopy, or photometry. Figure 11 shows the relationship between the resulting metallicity differences (present - reference) and the star clusters' ages. We restricted to reference $[Fe/H]$ values lower than -0.5 dex, included their associated errors, so that to comply with the metallicity range of eq. (4). We used all clusters listed in Table 1, except NGC 1795 and SL 817. The point sizes are proportional to N_{cls} , while their error bars come from adding in quadrature the uncertainties of the reference (Table B.1) and present mean $[Fe/H]$ values included in Table 1. The points are colored according to the N_{field}/N_{cls} ratios. Figure 11 reveals that the Strömgren metallicities derived from eq.(4) are age-dependent, and therefore, they need to be corrected for further use. A general trend is readily visible, which points of the need of discarding some individual discrepant $[Fe/H]$ values. In order to have a second reference source, we used the $[Fe/H]$ values derived from Strömgren theoretical isochrones (Bressan et al. 2012, $Y = 0.2485 + 1.78Z$, $Z_{\odot} = 0.0152$) to superimpose them onto Figure 11 (open magenta diamonds). We first built V vs. $(v - y)_0$ and V vs. m_{10} CMDs for $[Fe/H] = -2.0, -1.5, -1.0, -0.5,$ and 0.0 dex and $\log(\text{age}/\text{yr})=10.10$, which we called standard giant branches. We only drew the red giant branch track sections of these five theoretical isochrones. Then, we superimposed onto these standard giant branches the theoretical red giant branches of isochrones with $\log(\text{age}/\text{yr}) = 9.0$ and the five $[Fe/H]$ values as for $\log(\text{age}/\text{yr})=10.10$ (see Figure 12). Because of the age-metallicity degeneracy, the $\log(\text{age}/\text{yr})=9.0$ red giant branches appear shifted toward bluer colors with respect to the corresponding standard red giant branches according to their metallicities. We estimated by interpolating in the five stan-

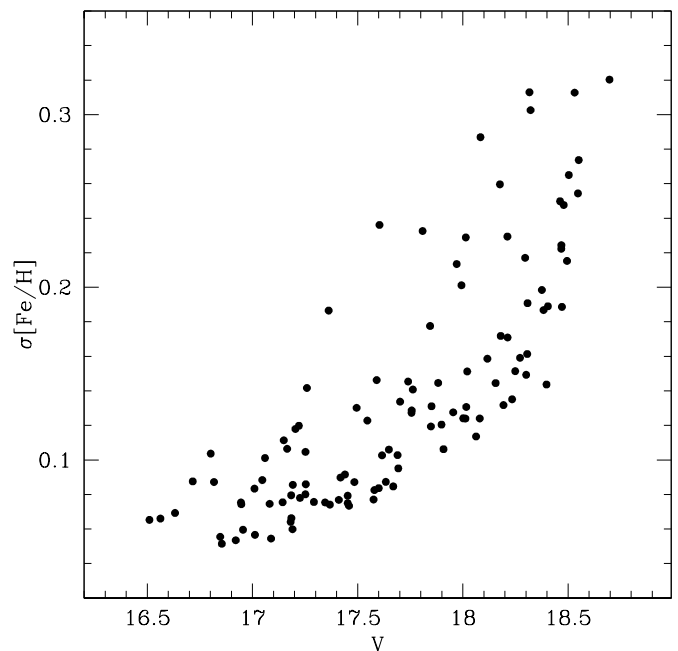


Fig. 9. Individual metallicity errors as a function of the V magnitude of stars selected in star cluster, represented by red large filled circles in Figures 1-8.

dard giant branches, the $[Fe/H]$ values of the $\log(\text{age}/\text{yr})=9.0$ red giant branches, and computed the difference between the obtained interpolated $[Fe/H]$ values and those given by the respective isochrones ($[Fe/H] = -2.0, -1.5, -1.0, -0.5,$ and 0.0 dex). We repeated this procedure for $\log(\text{age}/\text{yr})=9.4$ and 9.8 . By using these theoretical points and the general trend observed in Figure 11, we adopted weighted mean $[Fe/H]$ values for each cluster (see Table 1). Figure 13 depicts the resulting distribution using the adopted mean metallicities.

With the aim of providing with an expression for the metallicity correction that covers a wide age range, we added ten LMC old globular clusters studied by Piatti & Koch (2018) from Strömgren photometry. We took from that study the star clusters' ages and both reference and Strömgren metallicities, with their respective uncertainties. They are represented in Figures 11 and 13 with open circles. When performing a least square fit to all the data points, we obtained the following expression:

$$\Delta[Fe/H] \text{ (dex)} = -41.80(\pm 43.48) + 8.11(\pm 9.00) \times \log(\text{age}/\text{yr}) - 0.39(\pm 0.46) \times \log(\text{age}/\text{yr})^2,$$

with a standard deviation, a correlation factor, and an F-test coefficient of 0.05, 0.98, and 0.97, respectively. Strömgren metallicities calculated from eq.(4) should be corrected by an amount equal to $-\Delta[Fe/H]$.

5. Summary

Based on our previous knowledge that metallicities derived from standard giant branches in several photometric systems are affected by the age-metallicity degeneracy for star clusters younger than the old globular clusters, and bearing in mind the fundamental role that metallicities play in our understanding of the formation and chemical evolution processes at different Universe's scales, we decided to investigate it for the Strömgren vby

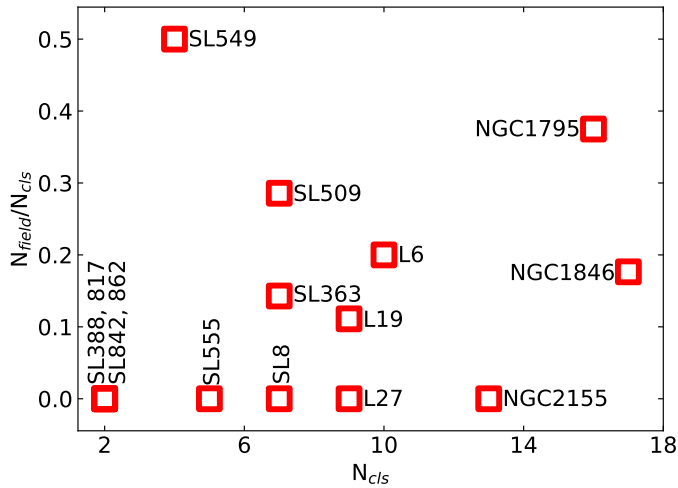


Fig. 10. Ratio of the number of stars in the field and that in the star clusters versus the number of selected stars in each star cluster.

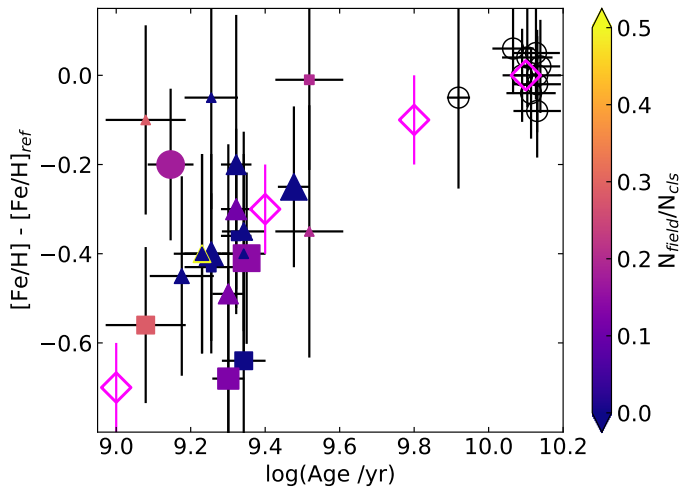


Fig. 11. Metallicity difference as a function of the star cluster's age. Filled circles, squares, and triangles correspond to high-resolution, low-resolution spectroscopy, and photometry reference values, respectively. Open magenta diamonds represent metallicity differences derived from theoretical isochrones (see text for details).

bandpasses. Until now, it has been straightforward to compute $[\text{Fe}/\text{H}]$ values from the Strömgren reddening free $(v-y)_0$ and m_{10} indices; the latter being a metallicity sensitive index. In general, they have been used for the study of globular cluster metallicity distributions (e.g., Calamida et al. 2014; Frank et al. 2015), to unveil multiple stellar populations (e.g., Carretta et al. 2011; Massari et al. 2016) rather than to estimate the metal content of intermediate-age star clusters.

In order to probe whether such an age dependence also affects the Strömgren metallicities, we made use of unexploited publicly available Strömgren vby images of intermediate-age and old LMC/SMC star clusters, which have been previously targeted for independent metallicity analysis. Once we properly proceeded the observational material and standardized the resulting instrumental photometry, we computed individual stellar $[\text{Fe}/\text{H}]$ values using the semi-empirical Calamida et al. (2007)'s calibration. We performed a sound selection of star cluster red giant branch candidates in order to comply with the metallicity calibration validity. In doing this, we constrained the cluster stars

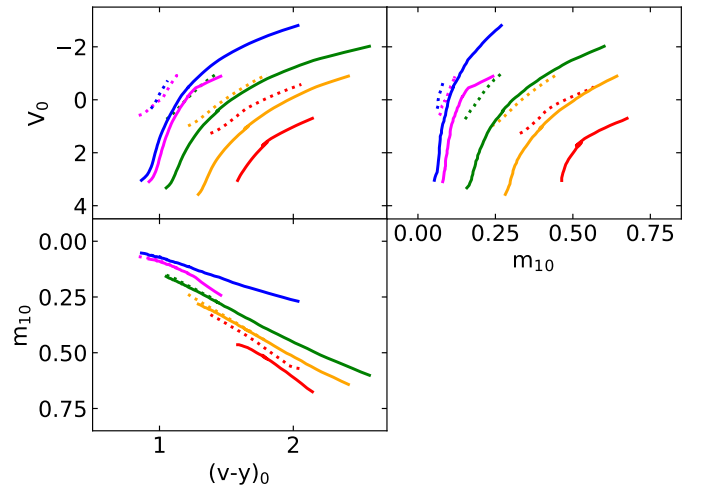


Fig. 12. Theoretical red giant branches for $\log(\text{age}/\text{yr})=9.0$ (dotted lines) and 10.10 (solid lines) and $[\text{Fe}/\text{H}] = -2.0, -1.5, -1.0, -0.5,$ and 0.0 dex shown with blue, magenta, green, orange, and red colors, respectively.

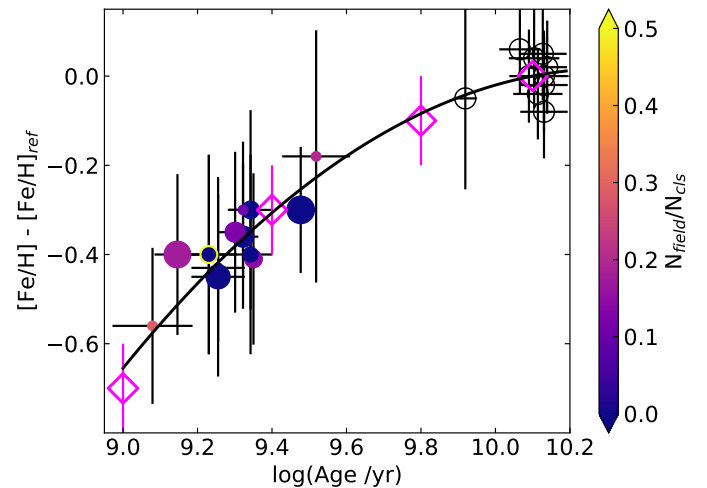


Fig. 13. Same as Figure 11 for adopted weighted mean $[\text{Fe}/\text{H}]$ values. The solid line represents the least squared fit obtained (see text for details).

to be distributed inside the star clusters' radii, located along the star cluster red giant branch, and with $[\text{Fe}/\text{H}]$ values within the readily visible star cluster metallicity range. We further assessed the effect in the derived mean star cluster metallicities of the contamination of field stars that are indistinguishable without proper motions or radial velocity measurements from the selected stars used to compute those mean values.

The resulting mean $[\text{Fe}/\text{H}]$ values and the estimated uncertainties were then compared with those metallicities taken from the literature. We found that the measured Strömgren metallicities need to be corrected by an amount that depends on the star cluster age, in the sense that, the younger the star cluster, the larger the metallicity correction. Since the measured $[\text{Fe}/\text{H}]$ values result more metal-poor than the reference $[\text{Fe}/\text{H}]$ ones, a positive correction should be added to the former one. From 26 relative metallicity points spanned from ~ 1 Gyr up to the globular cluster ages, we fitted a quadratically age-varying curve that provides with metallicity corrections with an overall uncertainty of

~ 0.05 dex. We finally repeated a similar comparison from a fully independent approach, which consisted in using theoretical red giant branches to trace the standard red giant branches and those of star clusters with ages in the aforementioned age range. Our findings show a very good agreement between the measured relative metallicities and those derived from theoretical isochrones.

Acknowledgements. I thank the referee for the thorough reading of the manuscript and timely suggestions to improve it.

References

- Adén, D., Feltzing, S., Koch, A., et al. 2009, *A&A*, 506, 1147
 Árnadóttir, A. S., Feltzing, S., & Lundström, I. 2010, *A&A*, 521, A40
 Bertelli, G., Nasi, E., Girardi, L., et al. 2003, *AJ*, 125, 770
 Bica, E., Bonatto, C., Dutra, C. M., & Santos, J. F. C. 2008, *MNRAS*, 389, 678
 Bica, E., Geisler, D., Dottori, H., et al. 1998, *AJ*, 116, 723
 Bressan, A., Marigo, P., Girardi, L., et al. 2012, *MNRAS*, 427, 127
 Calamida, A., Bono, G., Lagioia, E. P., et al. 2014, *A&A*, 565, A8
 Calamida, A., Bono, G., Stetson, P. B., et al. 2007, *ApJ*, 670, 400
 Calamida, A., Bono, G., Stetson, P. B., et al. 2009, *ApJ*, 706, 1277
 Carretta, E., Bragaglia, A., Gratton, R., D’Orazi, V., & Lucatello, S. 2011, *A&A*, 535, A121
 Correnti, M., Goudfrooij, P., Kalirai, J. S., et al. 2014, *ApJ*, 793, 121
 Crawford, D. L. & Mandwewala, N. 1976, *PASP*, 88, 917
 Da Costa, G. S. & Armandroff, T. E. 1990, *AJ*, 100, 162
 Dirsch, B., Richtler, T., Gieren, W. P., & Hilker, M. 2000, *A&A*, 360, 133
 Frank, M. J., Koch, A., Feltzing, S., et al. 2015, *A&A*, 581, A72
 Frogel, J. A., Cohen, J. G., & Persson, S. E. 1983, *ApJ*, 275, 773
 Geisler, D., Piatti, A. E., Bica, E., & Clariá, J. J. 2003, *MNRAS*, 341, 771
 Geisler, D. & Sarajedini, A. 1999, *AJ*, 117, 308
 Glatt, K., Grebel, E. K., & Koch, A. 2010, *A&A*, 517, A50
 Goudfrooij, P., Girardi, L., Kozhurina-Platais, V., et al. 2014, *ApJ*, 797, 35
 Grocholski, A. J., Cole, A. A., Sarajedini, A., Geisler, D., & Smith, V. V. 2006, *AJ*, 132, 1630
 Gruyters, P., Casagrande, L., Milone, A. P., et al. 2017, *A&A*, 603, A37
 Hartwick, F. D. A. 1968, *ApJ*, 154, 475
 Hauck, B. & Mermilliod, M. 1998, *A&AS*, 129, 431
 Hill, A. & Zaritsky, D. 2006, *AJ*, 131, 414
 Kerber, L. O., Santiago, B. X., & Brocato, E. 2007, *A&A*, 462, 139
 Leonardi, A. J. & Rose, J. A. 2003, *AJ*, 126, 1811
 Lindsay, E. M. 1958, *MNRAS*, 118, 172
 Massari, D., Lapenna, E., Bragaglia, A., et al. 2016, *MNRAS*, 458, 4162
 Mucciarelli, A., Carretta, E., Origlia, L., & Ferraro, F. R. 2008, *AJ*, 136, 375
 Olszewski, E. W., Schommer, R. A., Suntzeff, N. B., & Harris, H. C. 1991, *AJ*, 101, 515
 Ordoñez, A. J. & Sarajedini, A. 2015, *AJ*, 149, 201
 Palma, T., Gramajo, L. V., Clariá, J. J., et al. 2016, *A&A*, 586, A41
 Parisi, M. C., Grocholski, A. J., Geisler, D., Sarajedini, A., & Clariá, J. J. 2009, *AJ*, 138, 517
 Paunzen, E. 2015, *A&A*, 580, A23
 Piatti, A. E. 2011a, *MNRAS*, 416, L89
 Piatti, A. E. 2011b, *MNRAS*, 418, L40
 Piatti, A. E. 2018, *ArXiv e-prints* [[arXiv:1809.08123](https://arxiv.org/abs/1809.08123)]
 Piatti, A. E. & Bailin, J. 2019, *AJ*, 157, 49
 Piatti, A. E. & Bastian, N. 2016, *MNRAS*, 463, 1632
 Piatti, A. E., Bica, E., Geisler, D., & Clariá, J. J. 2003, *MNRAS*, 344, 965
 Piatti, A. E. & Koch, A. 2018, *ApJ*, 867, 8
 Piatti, A. E., Pietrzyński, G., Narloch, W., Górski, M., & Graczyk, D. 2019, *MNRAS*, 483, 4766
 Piatti, A. E., Sarajedini, A., Geisler, D., Seguel, J., & Clark, D. 2005, *MNRAS*, 358, 1215
 Pieres, A., Santiago, B., Balbinot, E., et al. 2016, *MNRAS*, 461, 519
 Rich, R. M., Shara, M. M., & Zurek, D. 2001, *AJ*, 122, 842
 Sarajedini, A. 1998, *AJ*, 116, 738
 Sarajedini, A., Grocholski, A. J., Levine, J., & Lada, E. 2002, *AJ*, 124, 2625
 Schlafly, E. F. & Finkbeiner, D. P. 2011, *ApJ*, 737, 103
 Shapley, H. & Lindsay, E. M. 1963, *Irish Astronomical Journal*, 6, 74
 Sharma, S., Borissova, J., Kurtev, R., Ivanov, V. D., & Geisler, D. 2010, *AJ*, 139, 878
 Song, Y.-Y., Mateo, M., Mackey, A. D., et al. 2019, *MNRAS*, 490, 385
 Stetson, P. B., Davis, L. E., & Crabtree, D. R. 1990, in *Astronomical Society of the Pacific Conference Series*, Vol. 8, *CCDs in astronomy*, ed. G. H. Jacoby, 289–304
 Stetson, P. B. & Harris, W. E. 1988, *AJ*, 96, 909
 Werchan, F. & Zaritsky, D. 2011, *AJ*, 142, 48
 Woo, J.-H., Gallart, C., Demarque, P., Yi, S., & Zoccali, M. 2003, *AJ*, 125, 754

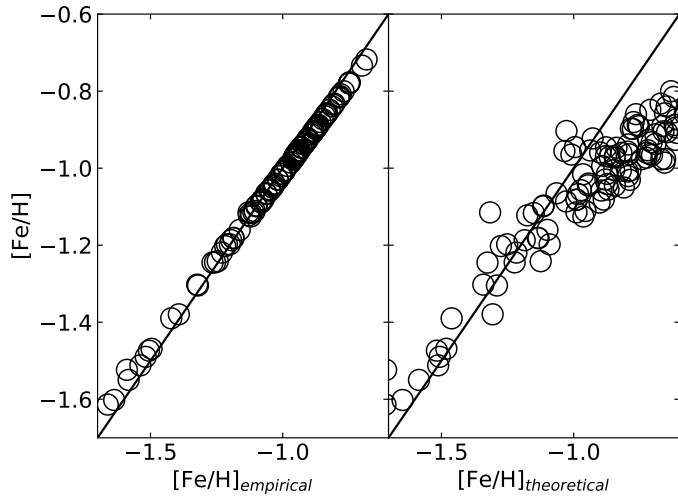


Fig. A.1. $[\text{Fe}/\text{H}]$ values from eq. 4 compared with those obtained from the empirical (left panel) and the theoretical (right panel) calibrations of Calamida et al. (2007). The solid line represents the identity relationship.

Appendix A: $[\text{Fe}/\text{H}]$ values based on Calamida et al. (2007)'s calibrations

For the sake of the reader, we present here a comparison between metallicities derived from different Calamida et al. (2007)'s calibrations, namely: empirical, theoretical, and semi-empirical (eq. 4) ones. As can be seen in Figure A.1, metallicities derived with the empirical or semi-empirical calibrations agree quite well. However, metallicities derived with the theoretical calibration are systematically more metal-poor compared to metallicities derived with the empirical and semi-empirical calibrations for $[\text{Fe}/\text{H}] > -1.0$ dex.

Appendix B: Cluster metallicities

We searched the literature looking for metallicity estimates for the cluster sample. Because of the relatively low brightness and small angular size of some clusters, photometric estimates were more frequently found, although some low-resolution spectroscopy values and other few high-spectroscopy ones were found. When comparing between them we found in some cases a significant dispersion, independently of the observational technique used (details are at the bottom of Table B.1), which prevented us to favor any particular technique. In order to adopt weighted mean values, we considered the whole collection of $[\text{Fe}/\text{H}]$ values (see Figure 11), which allowed us to recognize a general trend, and therefore to discard some visibly discrepant metallicities. We would like to note that possible sources of uncertainty due to different studies using different metallicities scales might exist.

Appendix C: Color-color diagram of the studied clusters

For the sake of the reader, Figure C.1 shows the m_{10} vs. $(v-y)_0$ diagrams with the positions of the selected stars in the studied LMC and SMC clusters.

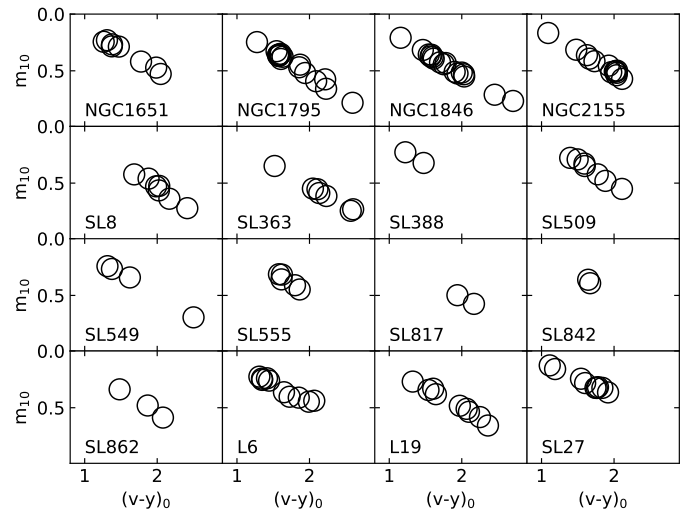


Fig. C.1. Color-color diagram of the selected stars (red filled circles in Figures 1-8).

Table B.1. [Fe/H] values for the cluster sample.

Star cluster	[Fe/H]	Reference	Star cluster	[Fe/H]	Reference	Star cluster	[Fe/H]	Reference
NGC 1651	-0.37±0.20	1	SL 8	-0.40±0.20	14	SL 862	-0.47±0.07	15
	-0.82±0.44	2		-0.50±0.30	20		-0.85±0.20	14
	-0.07±0.10	3	SL 363	-0.49±0.12	15	L 6	-1.24±0.03	17
	-0.63 to -0.45	4					-0.90±0.20	18
	-0.30±0.03	5				L 19	-0.75±0.10	18
	-0.70±0.10	6					SL 388	-0.65±0.20
NGC 1795	-0.40±0.10	12	-0.58±0.06	21	L 27	-1.14±0.06		17
	-0.23±0.20	1	SL 509	-0.54±0.09		15	-1.30±0.30	18
	NGC 1846	-0.50±0.10		13	-1.18±0.09	21	SL 549	-0.70±0.20
-0.76±0.20		1	-0.85±0.30	20				
-0.70±0.08		19	SL 555	-0.70±0.20	16			
NGC 2155	-0.55±0.20	1		SL 817	-0.41±0.05	15		
	-0.60±0.20	7			-0.50±0.20	14		
	-0.98 to -0.80	8		SL 842	-0.60±0.20	14		
	-0.44±0.86	2			-0.36±0.20	1		
	~-0.80	9			SL 842	-0.60±0.20	14	
	~-0.70	10	-0.36±0.20			1		
~-1.0	11	SL 842	-0.60±0.20	14				
-0.70±0.10	6		-0.36±0.20	1				

Reference (technique) : (1) Olszewski et al. (1991) (low-resolution spectroscopy); (2) Leonardi & Rose (2003) (integrated spectroscopy); (3) Sarajedini et al. (2002) (NIR photometry); (4) Dirsch et al. (2000) (Strömgren photometry); (5) Mucciarelli et al. (2008) (high-resolution spectroscopy); (6) Kerber et al. (2007) (HST photometry); (7) Rich et al. (2001) (HST photometry); (8) Bertelli et al. (2003) (VLT photometry); (9) Piatti et al. (2003) (Washington photometry); (10) Woo et al. (2003) (VLT photometry); (11) Sarajedini (1998) (HST photometry); (12) Glatt et al. (2010) (BVI photometry); (13) Grocholski et al. (2006) (low-resolution spectroscopy); (14) Bica et al. (1998) (Washington photometry); (15) Sharma et al. (2010) (low-resolution spectroscopy); (16) Geisler et al. (2003) (Washington photometry); (17) Parisi et al. (2009) (low-resolution spectroscopy); (18) Piatti et al. (2005) (Washington photometry); (19) Song et al. (2019) (high-resolution spectroscopy); (20) Palma et al. (2016) (Washington photometry); (21) Pieres et al. (2016) (DES photometry).